Spin dynamics of Fe_3Si and $Fe_{3-x}Mn_x$ alloys

1991 J. Phys.: Condens. Matter 3 4005

(http://iopscience.iop.org/0953-8984/3/22/012)

J. Phys.: Condens. Matter 3 (1991) 4005–4026. Printed in the UK

Spin dynamics of Fe_3Si and $Fe_{3-x}Mn_x$ alloys

M Szymańskit, M Jankowskit, L Dobrzyńskit, A Wiśniewski§ and S Bednarski¶

† Institute of Experimental Physics, Warsaw University, Hoża 69, 00–681 Warsaw, Poland

‡ Faculty of Physics, Warsaw University Branch, Lipowa 41, 15–424 Białystok, Poland

§ Institute of Physics, Polish Academy of Sciences, Al. Lotników 32/46, 02–668 Warsaw, Poland

¶ Institute of Atomic Energy, 05–400 Otwock-Świerk, Poland

Received 2 July 1990, in final form 23 January 1991

Abstract. The spin dynamics of the alloys Fe_3Si and $Fe_{3-x}Mn_xSi$, as studied by means of neutron inelastic scattering, has been analysed in terms of the Heisenberg model. In calculating the spin-wave dispersion relations for the DO_3-type structure, interactions up to the eighth-nearest neighbours were considered. It has been shown that the spin-wave dispersion relations in Fe_3Si, measured by Ziebeck and Forsyth throughout the whole Brillouin zone, cannot be described by less than three exchange integrals. On the other hand, there exists a strong correlation between the parameters fitted, so it is hard to choose an unambiguous set of exchange integrals describing the spin dynamics of this alloy. The spin-wave stiffness constant D of the alloy $Fe_{2.48}Mn_{0.52}Si$ was determined from neutron scattering measurements to be 95 ± 3 meV Å^2 and 110 ± 10 meV Å^2 at 293 K and 77 K, respectively. These results supplement our earlier measurements of $D(x)$ in the $Fe_{3-x}Mn_xSi$ system. From the concentration dependence of the stiffness constant the effective exchange integrals were estimated to be $J_{\rm eff}(0) = 25.2 \pm 0.7$ meV, $J^{\rm eff}_{\rm Fe-Mn} = 8.9 \pm 3.5$ meV and $J^{\rm eff}_{\rm Mn-Mn} = 0.1 \pm 1.1$ meV. The energy linewidths, $\Gamma(q)$, of the magnon peaks observed in $Fe_{2.48}Mn_{0.52}Si$ have been calculated assuming a Lorentzian form of the neutron scattering cross section. Within the range of magnon energies of 1 to 10 meV the $\Gamma(q)$ dependence is well reproduced by the theoretical result of Brooks Harris.

1. Introduction

The properties of Fe_3Si-based alloys with a DO_3-type structure have been a subject of intensive investigations, which were reviewed for the first time by Niculescu *et al* [1]. These authors demonstrated a number of properties like the structure, magnetic moments, hyperfine fields etc, which are strongly impurity and concentration dependent. There are a few remarkable features of these alloys which should be pointed out. The first is the selective occupation of sites when iron is substituted by various impurities. In particular, it was found that the impurities to the right of iron in the Periodic Table of the elements occupy so-called A sites, whereas impurities to the left of iron tend to occupy B sites. In order for the present paper to be as complete as possible, we present the DO_3 structure in figure 1; we also recall that the nearest surrounding of the A site in Fe_3Si consists of four iron atoms and four silicon atoms (D sites), while the nearest surrounding of the B site is the same as in BCC iron. Thus the symmetry of the latter

0953-8984/91/224005+22$03.50

site is cubic, whereas the former is tetrahedral. The other interesting feature of the alloys in question is a strong dependence of magnetic moments and hyperfine fields of iron on the number of nearest-neighbour (NN) iron atoms. The principal conclusion of [1] was that the magnetic properties of Fe_3Si-based alloys can be understood within a model in which only nearest-neighbour interactions are considered. Such a local model approach is very attractive indeed, though it certainly requires confirmation by a more direct investigations of basic interactions.

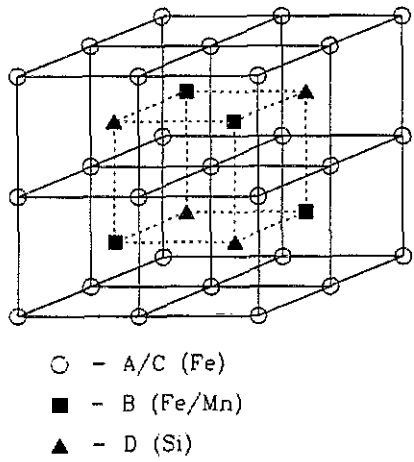

Figure 1. Unit cell of the DO_3-type structure with indication of site occupation for $Fe_{3-x}Mn_xSi$ alloys. The equivalent A and C sites are both referred to in the text as A sites.

Table 1. Neighbour configurations of A and B sites in Fe_3Si. The D sites are occupied by non-magnetic Si atoms, the Mn impurities tend to occupy B sites. The neighbour distance r_n/a is expressed in the units of lattice constant $a = 5.655$ Å.

Shell No	1	2	3	4	5	6	7	8
r_n/a	0.433	0.5	0.707	0.829	0.866	1	1.090	1.118
A	4B 4D	6A	12A	12B 12D	8A	6A	12B 12D	24A
B	8A	6D	12B	24A	8D	6B	24A	24D

The preferential occupation of B sites offers the unique possibility of measuring the impurity-matrix atom interactions at relatively high impurity concentrations, for the interaction with another impurity requires communication with the third-nearest-neighbour shell in which this impurity can be found (see table 1). If the nearest-neighbour interaction model were correct, such an interaction could be totally neglected. In fact, this was the primary motivation for undertaking the programme of systematic spin-wave investigations in $Fe_{3-x}Mn_xSi$ alloys [2–4].

Our interest in studying $Fe_{3-x}Mn_xSi$ alloys stems from other facts too. We know from diffuse neutron scattering experiments in disordered alloys $Fe_{1-c}Mn_c$ [5,6] that the magnetic moment of Mn varies with manganese concentration from about $-0.8\mu_B$

at $c = 0.0079$ to $+0.8\mu_B$ at $c \geq 0.03$. The magnetic moment of manganese which enters B sites in Fe_3Si is $\approx 2.2\mu_B$, as determined from neutron diffraction studies [7]. Because the nearest-neighbour configuration of the B site is identical to that found in iron, the difference in the band structures in these two cases must play a decisive role in the formation of the magnetic moment. In such a situation it would be surprising if the magnetic moment of Mn were sensitive to only the nearest-neighbour configuration.

The average magnetic moment of $Fe_{3-x}Mn_xSi$ alloys falls almost linearly with increasing Mn concentration for $x \leq 0.75$ [8]. Above this concentration, the manganese atoms start to occupy A sites and the situation appears to evolve as follows. The magnetic moment of the B site, which at $x < 0.75$ was nearly constant, decreases quickly with increasing x, and a characteristic dip in the temperature dependence of the magnetization is noticed when a sample is cooled down. Below about the liquid-nitrogen temperature the magnetization starts to decrease and the saturation magnetization at liquid-helium temperature is roughly 10% smaller than extrapolated from the high-temperature behaviour. In the neutron-diffraction pattern new diffraction maxima appear and these are interpreted by Yoon and Booth [8,9] as being due to the antiferromagnetic order among B sites, which become heavily or totally occupied by Mn atoms. An explanation for this behaviour has been sought in the antiferromagnetic Mn–Mn interaction between the second-nearest neighbours (which are separated by a distance equal to the lattice constant, which means that they occupy the sixth coordination sphere) and the ferromagnetic nearest-neighbour interaction (with atoms from the third coordination sphere). On the other hand, the temperature dependence of the magnetic moment distribution of Mn in disordered Fe–Mn alloys [10–12] indicates that the Mn moment is relatively weakly bound to the iron lattice, which results in its rapid decrease with temperature. At the same time the average magnetic moment of iron changes slowly. A similar trend was also postulated in recent studies of $Fe_{3-x}Mn_xSi$ alloys [13]. Nakai and Kunitomi [10] try to explain this behaviour through the small (< 0.1) ratio of the Fe–Mn and Fe–Fe exchange integrals. This indicates that a direct search for the exchange integrals is necessary for an understanding of the phenomenon described above.

We also initiated studies of the $Fe_{3-x}Al_x(Si_{1-y}Al_y)$ system and the essential facts worth mentioning in connection with our studies of exchange interactions are the following. It has been known for many years that Fe_3Al alloys with some excess of aluminium, more precisely in the composition range close to $Fe_{0.7}Al_{0.3}$, exhibit a series of non-standard phase transitions, starting from a paramagnetic phase at high temperature, to a ferromagnetic state at lower temperature, then reentering the paramagnetic phase again and ending in the spin-glass phase [14]. This behaviour was explained by Motoya *et al* [15], based on neutron scattering studies, as being due to the presence of random fields which in turn arise from competing ferromagnetic interactions among the iron NN and antiferromagnetic interactions between the second-NN. The presence of such random fields may also be a reason for the apparent broadening of the Mössbauer spectra observed by Huffman [16]. Although such a series of unusual phase transitions was not observed in similar Fe–Si alloys, the Mössbauer spectra of $Fe_{3-x}Al_xSi$ alloys with $x \leq 0.3$ showed line broadening and the presence of a low-field component which could be attributed to the random fields [17]. The reason for there being such a different situation in Fe_3Si-based and Fe_3Al-based alloys may be regarded as being due to the rather large difference in the lattice constants of both alloys: 5.65 Å in Fe_3Si and about 5.80 Å in Fe_3Al. The larger atomic separation in Fe_3Al should in principle lead to narrower bands and thus to more localized behaviour

of the magnetic moments. This can also influence the exchange couplings. Indeed, as was shown by Dobrzyński *et al* [18], the effective exchange interaction varies strongly with the lattice constant in the Fe_3Si–Fe_3Al system with DO_3-type structure, whereas it is weakly dependent on the interatomic distance in the disordered Fe–Al–Si alloys. In particular, from this work one can expect that the exchange interaction between second-nearest neighbours can be negative which would match the requirements of the random-field model well. However, despite the relatively broad energy range of spin-wave excitations studied in Sendust ($Fe_{2.94}Al_{0.38}Si_{0.68}$) [19], antiferromagnetic interactions were not convincingly found. These facts challenge one to undertake more detailed investigations of the exchange interactions in this system.

We discuss here the spin dynamics of Fe_3Si and $Fe_{3-x}Mn_xSi$ ($x \leq 0.6$). The spin dynamics is analysed mainly in terms of the Heisenberg model, although we have no doubts that there is a need to work out the band model.

The paper is organized as follows. In section 2 the calculations of the spin-wave dispersion relations in DO_3-type structure are presented. Because the long-range interactions can be important, we consider the Heisenberg model with interactions up to the eighth-nearest neighbours. In section 3 this model is used for interpretation of spin-wave dispersion relations in Fe_3Si. The experimental results obtained for $Fe_{3-x}Mn_xSi$ alloys are reviewed in section 4. Finally, in section 5 we discuss the physical information brought by these results and present our conclusions.

2. Spin-wave theory

The spin-wave dispersion relations in the DO_3-type system were calculated for the first time by Leoni and Natoli [20] in the approximation of nearest- and next-nearest-neighbour interactions. This approximation, however, is too poor for our purposes and we therefore extended the Leoni and Natoli approach to the case of interactions with neighbours up to and including the eighth coordination sphere.

Following the ideas of Leoni and Natoli, the Holstein–Primakoff transformation applied to the Heisenberg Hamiltonian

$$\mathcal{H} = -\sum_{\beta\gamma}\sum_{ij} J_{ij}^{\beta\gamma} \boldsymbol{S}_{\beta i}\boldsymbol{S}_{\gamma j} \tag{1}$$

where β and γ denote the magnetic sublattices (A, B and C), leads to the following Hamiltonian quadratic in creation and annihilation operators $b_{k\gamma}^{+}, b_{k\gamma}$:

$$\mathcal{H}_Q = 2\sum_{k}\sum_{\beta\gamma}\Big(S_\beta \sum_j J_{\beta\gamma}(\boldsymbol{r}_{0\beta} - \boldsymbol{r}_{j\gamma}) b_{k\gamma}^{+} b_{k\gamma} - \sqrt{S_\beta S_\gamma}\sum_j J_{\beta\gamma}(\boldsymbol{r}_{0\beta} - \boldsymbol{r}_{j\gamma}) \exp[-\mathrm{i}\boldsymbol{k}(\boldsymbol{r}_{0\beta} - \boldsymbol{r}_{j\gamma})] b_{k\beta} b_{k\gamma}^{+} + \mathrm{cc}\Big). \tag{2}$$

For symmetry reasons we assume $S_A = S_C$ and $J_{\alpha A} = J_{\alpha C}$. This Hamiltonian is easily diagonalized for $\boldsymbol{k}$ along [100] or [110] directions with help of the following symmetry coordinates:

$$\begin{aligned} \xi_1 &= b_{kB} \\ \xi_2 &= (1/\sqrt{2})\,(b_{kA} + b_{kC}) \\ \xi_3 &= (1/\sqrt{2})\,(b_{kA} - b_{kC}) \end{aligned} \tag{3}$$

which modify $\mathcal{H}_Q$ to

$$\mathcal{H}_Q = a_3\xi_3^\dagger\xi_3 + 2a_1\xi_1^\dagger\xi_1 + 2a_2\xi_2^\dagger\xi_2 - a_{12}\left(\xi_1\xi_2^\dagger + \xi_2\xi_1^\dagger\right). \tag{4}$$

The values of the coefficients a_1, a_2, a_{12} and a_3 for the [100] and [110] directions may be found in appendix A.

The spin-wave energies are given by

$$\begin{aligned}\omega_{1,2} &= a_1 + a_2 \pm \sqrt{(a_1 - a_2)^2 + a_{12}^2} \\ \omega_3 &= a_3\end{aligned} \tag{5}$$

where apparently the solution ω_1 with $(-)$ sign describes the lowest-lying mode, or 'acoustic' spin-wave branch, which at low values of wavevector, $ka \ll 1$, has the form

$$\omega_1 \approx Dk^2 \tag{6}$$

with the exchange stiffness constant D given by

$$D = \frac{S_A S_B j_{AB} + S_A^2 j_{AA} + 2S_B^2 j_{BB}}{2S_A + S_B} a^2 \tag{7}$$

where j_{AB}, j_{AA} and j_{BB} are 'effective' exchange integrals between atoms on respective sublattices

$$\begin{aligned} j_{AB} &= J_{AB}(1) + 11J_{AB}(4) + 19J_{AB}(7) \\ j_{AA} &= J_{AA}(2) + 4J_{AA}(3) + 4J_{AA}(5) + 4J_{AA}(6) + 20J_{AA}(8) \\ j_{BB} &= J_{BB}(3) + J_{BB}(6). \end{aligned} \tag{8}$$

Here $J_{\alpha\beta}(n)$ denotes the exchange integral between the nth-nearest neighbours, one of which is located at the α site while the other resides at the β site. Of course, an identical expression for D is obtained for an arbitrary direction of the wavevector $\boldsymbol{k}$.

To obtain dispersion relations along the [111] direction one should solve the third-order equation

$$\begin{vmatrix} a_{11} - \omega & a_{12} & a_{13} \\ a_{12}^* & a_{22} - \omega & a_{12} \\ a_{13} & a_{12}^* & a_{11} - \omega \end{vmatrix} = 0 \tag{9}$$

which although in principle is an easy task, in practice leads to expressions whose structure is not very easy to read. For the sake of completeness the forms of all the necessary coefficients are given in appendix A.

When an impurity M is substituted for iron, i.e. one deals with $Fe_{3-x}M_xSi$, the expressions for spin-wave energies should be modified in accordance with a change the impurity may introduce in both the local spin value and the exchange interactions. Within the mean-field (or average-crystal) approximation, when the impurity M locates randomly at the site B, which is the case of our particular interest, we can

still use the expression (7) for the exchange stiffness constant but with the following changes:

$$\begin{aligned} S_A S_B j_{AB} &\longrightarrow S_A S_B(1-x)j_{AB} + S_A S_M x j_{AM} \\ S_B^2 j_{BB} &\longrightarrow S_B^2(1-x)^2 j_{BB} + 2S_B S_M x(1-x)j_{BM} + S_M^2 x^2 j_{MM} \end{aligned} \tag{10}$$

where S_M denotes the impurity spin, the subscripts A and B concern iron at the A and B sites, respectively, and M denotes the impurity. In the considered case the expression for j_{AA} does not change.

Similarly, when the impurity substitutes for iron at the A sites one has to change

$$\begin{aligned} S_A^2 j_{AA} &\longrightarrow S_A^2(1-x/2)^2 j_{AA} + 2S_A S_M(x/2)(1-x/2)j_{AM} + S_M^2(x/2)^2 j_{MM} \\ S_A S_B j_{AB} &\longrightarrow S_A S_B(1-x/2)j_{AB} + S_B S_M(x/2)j_{BM} \end{aligned} \tag{11}$$

without changing j_{BB}.

Let us also define an effective exchange integral in the system by

$$J_{\text{eff}} = \frac{2S_A + S_B}{S_A S_B}\,\frac{D}{a^2}\,. \tag{12}$$

If the only important exchange interaction took place among the nearest neighbours, as suggested in [1], then J_{eff} would simply be the value characterizing this interaction. This parameter was shown in [18] to be strongly dependent on the lattice constant. This dependence, together with $J_{\text{eff}}/k_B T_C$, where T_C is the Curie temperature, is displayed in figure 2, in which we also included the values obtained from temperature dependence of magnetization, measured for Fe_3Ga [21]. It can be seen from this figure that when the distances between atoms decrease, the coupling between them becomes stronger. At the same time the Curie temperature is not so strongly affected. This can indicate that the itinerancy of magnetism becomes stronger with decreasing lattice constant. Indeed, such a situation can be expected on the elementary grounds of solid-state theory.

For the pure DO_3 structure, it follows from (7) that

$$J_{\text{eff}}(0) = j_{AB} + \left(\frac{S_A}{S_B}\right) j_{AA} + 2\left(\frac{S_B}{S_A}\right) j_{BB}\,. \tag{13}$$

One can easily check that for the impurities locating at B sites

$$\begin{aligned} J_{\text{eff}}(x) = (1-x)j_{AB} + \left(\frac{S_M}{S_B}\right) x j_{AM} + \left(\frac{S_A}{S_B}\right) j_{AA} + 2\left(\frac{S_B}{S_A}\right)\Big[(1-x)^2 j_{BB} \\ + 2\left(\frac{S_M}{S_B}\right) x(1-x)j_{BM} + \left(\frac{S_M}{S_B}\right)^2 x^2 j_{MM}\Big]\,. \end{aligned} \tag{14}$$

A particularly simple expression is obtained for the manganese impurity. As it was shown in [7], for $x < 0.75$ the manganese moment is hardly different from the iron moment at the B site, whereas in the same concentration range iron at the A site is losing its moment with a rate given approximately by

$$S_A(x) \approx S_A(0)(1-x)\,. \tag{15}$$

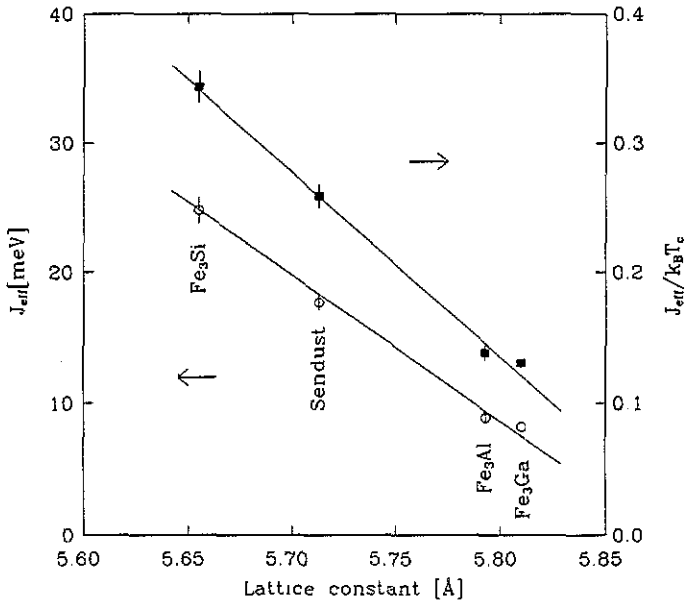

Figure 2. Dependence of the effective exchange integral J_{eff} and the ratio of J_{eff}/k_BT_C on the lattice constant a for ordered iron alloys with DO_3 structure.

In this approximation the J_{eff} can be expressed as

$$J_{\text{eff}}(x) = J_{\text{eff}}(0)(1-x) + xJ^{\text{eff}}_{\text{Fe-Mn}} + \left(\frac{x^2}{1-x}\right) 2\left(\frac{S_B}{S_A(0)}\right) J^{\text{eff}}_{\text{Mn-Mn}} \quad (16)$$

where

$$J^{\text{eff}}_{\text{Fe-Mn}} = J_{\text{Fe-Mn}}(1) + 11J_{\text{Fe-Mn}}(4) + 19J_{\text{Fe-Mn}}(7) + 4(S_B/S_A(0))(J_{\text{Fe-Mn}}(3) + J_{\text{Fe-Mn}}(6)) \quad (17)$$

$$J^{\text{eff}}_{\text{Mn-Mn}} = J_{\text{Mn-Mn}}(3) + J_{\text{Mn-Mn}}(6).$$

We hope that the abbreviations used in the above expressions are self-explanatory. The most important observation is that the effective Fe–Mn interaction can be obtained even without a detailed knowledge of the exchange interactions in Fe_3Si, because in this particular case the spin dynamics of the matrix alloy is represented in (16) by $J_{\text{eff}}(0)$ alone.

The use of the effective exchange integral (12) with S_A given by (15) is obviously limited to $x < 0.75$, because equation (15) holds only in this concentration range. On the other hand, with increasing manganese concentration the average-crystal approximation may worsen, and the result of such an approximation should be treated cautiously. Its main advantage lies in a plausible parametrization of the various exchange interactions taking place in DO_3-type mixed systems. Such clarity could hardly be achieved if the exchange stiffness constant were discussed instead of J_{eff}.

3. Exchange interactions in Fe_3Si

In order to study exchange interactions in Fe_3Si we have used unpublished results of

Ziebeck and Forsyth [22] that were obtained at the Institut Laue–Langevin, Grenoble. They have measured spin-wave dispersion relations along three principal symmetry directions over a wide energy range (up to 145 meV) and over a whole Brillouin zone. We have applied the extended formulae for dispersion relations that include interactions with neighbours up to and including the eighth coordination sphere (10 exchange integrals) to fit their experimental results. The minimization program MINUIT (CERNlib) has been used for this purpose. Because the experimental points lie on rather smooth curves (see figure 3), the attempted fitting of 10 parameters had to be performed gradually, starting from the lowest possible number of fitted parameters, and carefully checking the physical sense of the parameters obtained. The fit for all three directions has been done simultaneously, with the use of $N = 43$ experimental points. The quality of every fit is given by the value of the root-mean square (RMS) of the difference between calculated and measured values

$$\mathrm{RMS} = \left(\frac{1}{N} \sum_{i=1}^{N} \left(\omega_{\mathrm{exp}}(i) - \omega_{\mathrm{theo}}(i) \right)^2 \right)^{1/2} . \tag{18}$$

For each set of integrals the exchange stiffness constant D has been calculated. The values obtained ought to be compared with $D = 240 \pm 10$ meV Å^2 reported by Blanckenhagen and Lin [23]. The results of the fitting are presented in table 2 and illustrated in figure 3.

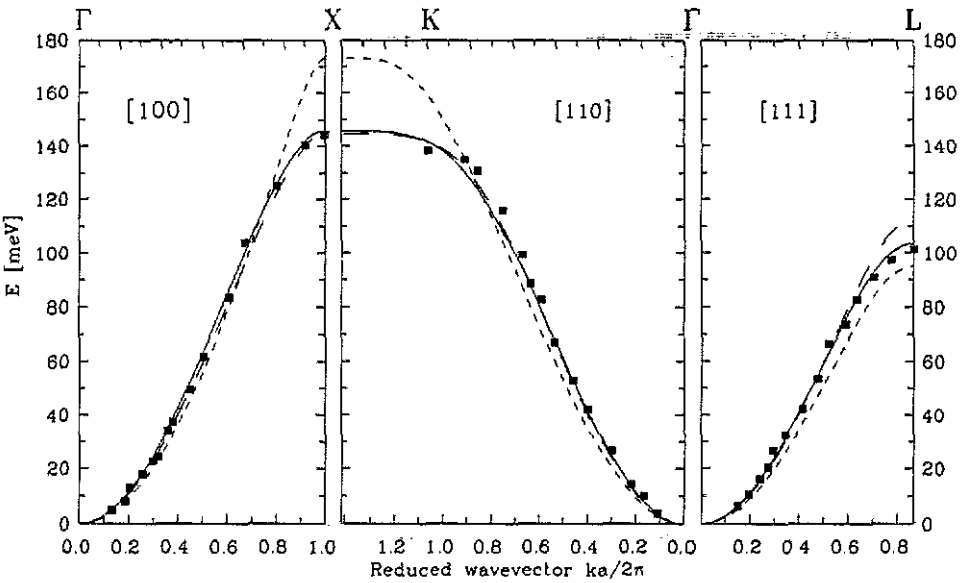

Figure 3. Spin-wave dispersion relation of Fe_3Si. The points are experimental results of Ziebeck and Forsyth [22], the lines represent the fits to the Heisenberg model with various ranges of interactions: – – –, interactions with first-nearest neighbours only; — — —, interactions with first- and second-nearest neighbours; ——, interactions up to third-nearest neighbours.

There is no doubt that neither nearest-neighbour interactions nor nearest-neighbour and next-nearest-neighbour interactions can explain the experimental re-

Table 2. Values of exchange integrals and stiffness constant of Fe_3Si obtained by fitting the Heisenberg model to the spin-wave dispersion relations measured by Ziebeck and Forsyth [22].

$J_{AB}(1)$ (meV)	$J_{AA}(2)$ (meV)	$J_{AA}(3)$ (meV)	$J_{BB}(3)$ (meV)	$J_{AB}(4)$ (meV)	D (meV Å^2)	RMS
19.7 ± 0.9					190	8.67
13.4 ± 0.1	15.5 ± 0.3				222	3.68
13.5 ± 0.1	3.4 ± 0.7	3.7 ± 0.2			240	2.71
16.0 ± 0.2	0.8 ± 0.2		2.6 ± 0.1		240	2.67
9.5 ± 0.3	0.9 ± 0.2	2.7 ± 0.1	2.7 ± 0.1		244	2.76
10.0	2.1 ± 0.3	2.4 ± 0.1	3.3 ± 0.3	-0.3 ± 0.1	241	2.56
20.0	1.5 ± 0.3	-1.6 ± 0.1	2.9 ± 0.3	-0.2 ± 0.1	238	2.51

sult. When three parameters are fitted, a problem arises as to what is the relation between AA and BB interactions, corresponding to the same (third-nearest-neighbour) distance between the atoms. In the third and fourth rows of table 2 the sets of exchange integrals fitted under the assumption that either $J_{AA}(3)$ or $J_{BB}(3)$ is zero are shown. Finally, the results presented in the fifth row were obtained under the assumption of $J_{AA}(3) = J_{BB}(3)$. In all three cases the quality of the fit is much the same and the calculated exchange stiffness constant is very close to the expected value $D = 240$ meV Å^2. Our attempts to fit more than three different exchange integrals turned out to be unsuccessful in the sense that addition of the next parameter resulted in a drastic change of the parameters previously found without a substantial improvement in the quality of the fit.

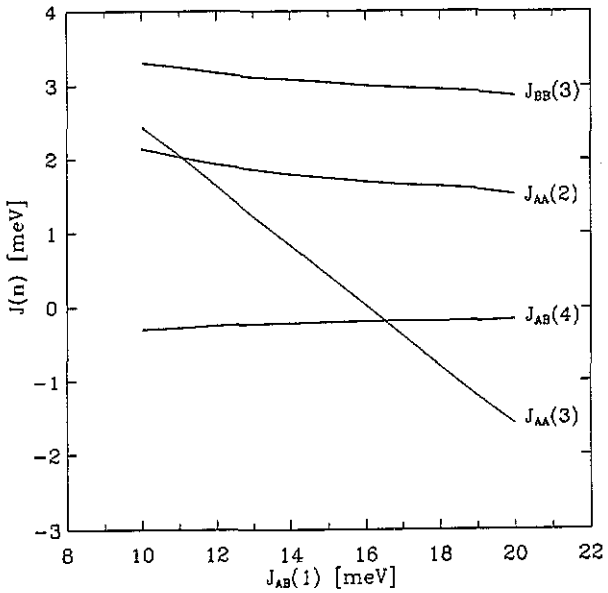

Figure 4. Exchange integrals $J_{AA}(2)$, $J_{AA}(3)$, $J_{BB}(3)$ and $J_{AB}(4)$ versus nearest-neighbour exchange integral $J_{AB}(1)$ determined from fitting the Heisenberg model to the experimental spin-wave dispersion relations of Fe_3Si.

Because of the strong correlation between parameters of the fit we found it useful to carry out the fittings with various values of $J_{AB}(1)$ kept fixed. In that way, by controlling consistency of the parameters resulting from the fit, one might hope that their number could effectively be increased. The values of $J_{AA}(2)$, $J_{AA}(3)$, $J_{BB}(3)$ and $J_{AB}(4)$ obtained from this procedure for $J_{AB}(1)$ varying from 10 to 20 meV are shown in figure 4. The quality of the fit and the values of D are almost the same in this range of $J_{AB}(1)$, as can be seen from table 2, where the results obtained for $J_{AB}(1)$ fixed at 10 and 20 meV are presented in the last two rows. For $J_{AB}(1) < 10$ meV the quality of the fit starts to decrease. On the other hand, in most of the earlier fits, carried out under various constraints, with $J_{AB}(1)$ treated as one of the variable parameters the values of $J_{AB}(1)$ obtained were smaller than 20 meV. So we can probably set this value as the upper limit of $J_{AB}(1)$. The main feature of the results presented in figure 4 is a strong linear correlation between $J_{AA}(3)$ and $J_{AB}(1)$ and a rather weak dependence of the other integrals on $J_{AB}(1)$.

The inclusion of interactions with neighbours from coordination spheres further away than the fourth allowed us to improve the quality of the fit substantially (down to RMS = 1.60). However, it resulted in a sequence of some unexpectedly high values of exchange integrals at large distances or in several equivalent local minima corresponding to definitely different sets of parameters. Apparently, the minimum RMS criterion is not a sufficient one for our case, which in practice limits to five the number of exchange integrals that can be inferred from the data. In this case one could say that the values of exchange integrals probably lie in a range defined by last two rows of table 2 and no criterion was found which could help to choose the best set of values. Therefore we tried to look for a possibly simple model which would indicate some sensible dependence of the exchange integrals on the distance.

With this goal in mind, the experimental results have been analysed in terms of the Caroli–Blandin modification [24] of the RKKY theory. The advantage of the model lies in a small number of fitted parameters which does not exceed four. However the attempts to fit the dispersion relations in the Caroli–Blandin approach were unsuccessful due to either non-physical meaning of the parameters obtained from the fits or just a poor quality of fit.

To conclude this section, one can say that the spin dynamics of Fe_3Si cannot be described by the Heisenberg model with short-range interactions, and at least the third-nearest neighbours should be taken into account. In order to parametrize the spin-wave dispersion relations accurately one should in fact use more parameters, but they cannot be drawn unambiguously from the available experimental results. In our opinion this situation calls for good band-model calculations.

4. Spin waves in $Fe_{3-x}Mn_xSi$ alloys

Studies of spin-wave dispersion relations in $Fe_{3-x}Mn_xSi$ alloys with $x = 0.04$, 0.18 and 0.32 by means of inelastic neutron scattering were reported in our earlier papers [2,3]. Those measurements were performed at room temperature and the values of the spin-wave stiffness constant $D_{RT}(x)$ were obtained after correction of the data for resolution effects, assuming no damping of spin waves.

At finite temperature the interactions between spin waves, leading to the renormalization of their energies, should be taken into account. For this reason the low-temperature values of the stiffness constant rather than the room-temperature ones are

needed for the correct evaluation of exchange interactions in $Fe_{3-x}Mn_xSi$ alloys. To rule out the effects of the renormalization of spin-wave energies the low-energy parts of the spin-wave dispersion relations were re-measured at liquid-nitrogen temperature for all the samples mentioned above [25]. The main conclusion was that the renormalization of the spin-wave constant between liquid-nitrogen and room temperature was relatively small. This point will be discussed further at the end of this section.

Below we describe the recent results obtained for $Fe_{2.48}Mn_{0.52}Si$ and present a more sophisticated method of data analysis which was also used to correct our earlier data for finite spin-wave lifetime.

4.1. Sample characterization

The sample was a large single crystal of dimensions (26 × 30 × 40) mm^3 with the long axis along $[1\bar{1}0]$ and the two other axes along [001] and [110]. It was spark cut from a roughly cylindrical boule grown by the Bridgman technique. Neutron diffraction measurements of (100), (220) and (111) Bragg reflections showed that the quality of the crystal was not very high (rather wide and slightly deformed profiles of Bragg peaks) but no significant twinning or presence of misoriented microcrystals was detected.

The Curie temperature $T_C = 497 \pm 4$ K and magnetic moment per formula unit $\mu = 3.25\mu_B$ at 4.2 K were obtained from the magnetization measurements, so the composition of the sample could be determined as $x = 0.52 \pm 0.02$ from the linear dependence of $T_C(x)$ and $\mu(x)$ in this range of x [9]. This composition was also confirmed by an electron microprobe scan [26].

4.2. Experimental details

The experiment was carried out on a TKSN-420 triple-axis neutron spectrometer at the EWA reactor in Świerk. Pyrolytic graphite crystals with mosaic spreads of 25′ and 60′ were used as monochromator and analyser, respectively, and the horizontal collimations were 30′–55′–55′–55′. The vertical divergences were estimated as 30′–45′–90′–90′ from the heights of all the crystals used and the distances between them. These parameters were subsequently used for calculation of the resolution function.

The crystal was mounted with its long $[1\bar{1}0]$ axis vertical, so the measurements of inelastic neutron scattering could be easily performed in the vicinity of (111), (220) or (002) reciprocal lattice points. A proper choice of the Bragg point for spin-wave studies should result in possibly strong magnetic scattering as well as relatively low nuclear phonon scattering in its vicinity. For the DO_3-type of structure only Bragg reflections with Miller indices either all odd or all even are allowed and there are three types of nuclear structure factors for neutron diffraction, namely

$$\begin{aligned} F_{111}^{nuc} &= b_B - b_D = b_{Fe/Mn} - b_{Si} \\ F_{200}^{nuc} &= b_B + b_D - 2b_A = b_{Fe/Mn} + b_{Si} - 2b_{Fe} \\ F_{220}^{nuc} &= b_B + b_D + 2b_A = b_{Fe/Mn} + b_{Si} + 2b_{Fe} . \end{aligned} \tag{19}$$

The first two are sublattice structure factors and the last is the fundamental one. For $Fe_{3-x}Mn_xSi$ alloys the substitution of Mn atoms in the B position changes the value of b_B only

$$b_B = xb_{Mn} + (1-x)b_{Fe} . \tag{20}$$

Table 3. Comparison of nuclear and magnetic structure factors of Fe_3Si and $Fe_{2.48}Mn_{0.52}Si$ alloys. For the calculation of magnetic factors the magnetic moments reported by Yoon and Booth [8,9] and the magnetic form factor of iron were used.

Crystal composition	Nuclear structure factors			Magnetic structure factors		
	$\|F^{nuc}_{111}\|^2$	$\|F^{nuc}_{200}\|^2$	$\|F^{nuc}_{220}\|^2$	$\|F^{M}_{111}\|^2$	$\|F^{M}_{200}\|^2$	$\|F^{M}_{220}\|^2$
Fe_3Si	0.29	0.29	10.9	0.22	0.002	0.52
$Fe_{2.48}Mn_{0.52}Si$	0.02	1.51	6.8	0.22	0.04	0.28

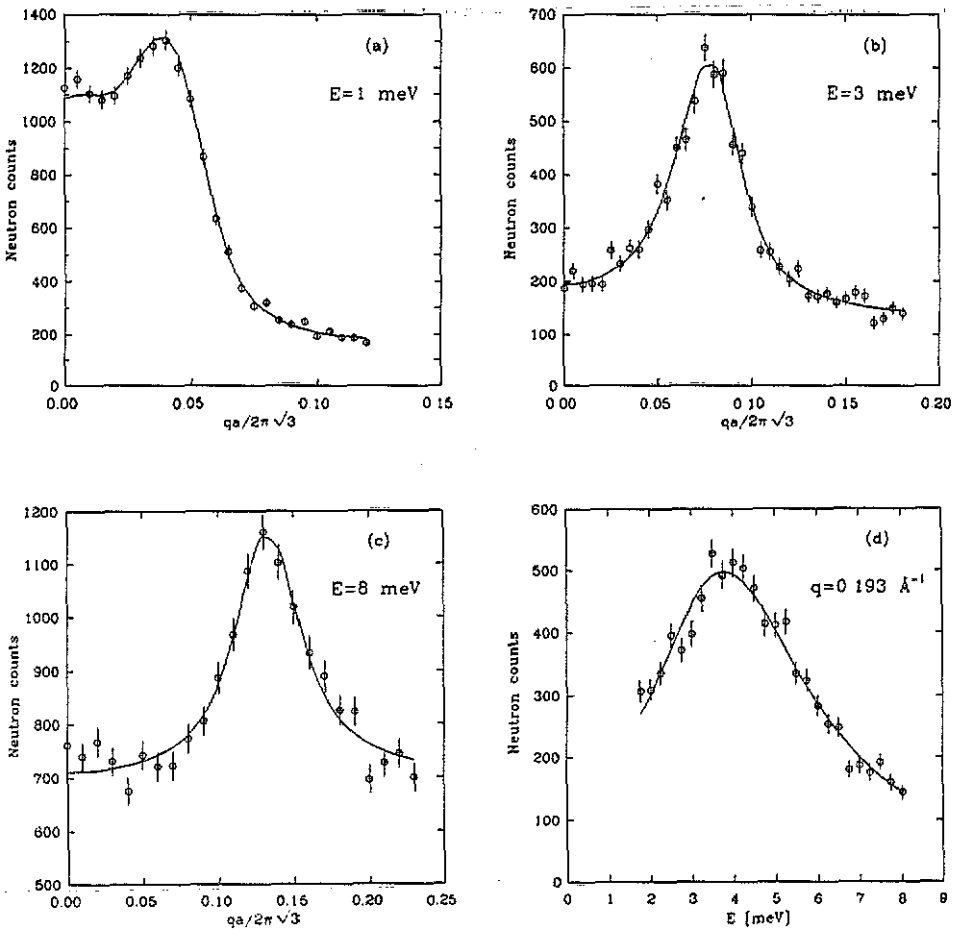

Figure 5. Typical examples of magnon peaks observed in: (*a*), (*b*) and (*c*) constant-E; (*d*) constant-Q scans at room temperature. The full curves correspond to the fits of the Lorentzian cross section convoluted with the instrumental resolution function.

As the scattering lengths of manganese and iron are of opposite sign the value of b_B decreases with growing Mn concentration leading to very low values of the nuclear structure factor F^{nuc}_{111}. At the same time, the magnetic structure factor F^{M}_{111}, which depends on the value of magnetic moment at the B site alone, is approximately in-

dependent of manganese concentration for $x < 0.75$. It is evident from (19) that relative changes of the structure factors (220) and (200) with x increasing are much less pronounced.

This behaviour is illustrated in table 3, where we compare the nuclear and magnetic structure factors of pure Fe_3Si and of our sample with $x = 0.52$. From table 3 it is obvious that magnon scattering of unpolarized neutrons from $Fe_{3-x}Mn_xSi$ should be studied in the Brillouin zone around the (111) reciprocal lattice point. Because of the very small value of the nuclear structure factor F_{111}^{nuc}, phonon scattering in the vicinity of this point may be neglected in comparison with magnon scattering. This situation is especially convenient for a crystal with significant degree of disorder in the lattice when peaks of inelastic scattering can be expected to be rather wide and difficult to divide into phonon and magnon parts. On the other hand, the fundamental (220) or (004) Bragg points with very large nuclear structure factor could be used as starting points for additional measurements of the acoustic phonon branches. According to the above conclusions the measurements of magnon scattering in our sample were performed around the (111) Bragg point with q parallel to the [111] direction.

The majority of measurements were made with the constant-E method in the neutron energy loss mode. In the first series of constant-E scans performed at room temperature the final neutron energy E_f was fixed at 16.9 meV. A similar series of scans, as well as additional constant-E and constant-Q scans, were made in the second series of measurements with $E_f = 14.9$ meV using a pyrolytic graphite (PG) filter to remove higher-order contaminations, which had been suspected to influence neutron spectra observed in the former series of scans. Nevertheless, both series of measurements provided very similar results. The measured magnon peaks for energy transfers greater than 10 meV were very diffuse and difficult to analyse quantitatively. In order to assess the renormalization of spin-wave energies at room temperature, some constant-E scans were also made at liquid-nitrogen temperature. They had to be limited to energy transfers $\Delta E \leq 8$ meV because of the very low intensity of the magnon peaks.

Some typical room-temperature scans, with energy transfers of 1, 3 and 8 meV and the momentum transfer of 0.193 Å^{-1} are shown in figure 5.

4.3. Data analysis

The observed neutron spectra represent a convolution of the actual neutron scattering cross section with the resolution function of the spectrometer $R(\Delta \boldsymbol{Q}, \Delta\omega)$

$$I(\boldsymbol{Q},\omega) = \int \frac{\mathrm{d}^2\sigma}{\mathrm{d}\omega\,\mathrm{d}\Omega}(\boldsymbol{Q}',\omega')R(\boldsymbol{Q}-\boldsymbol{Q}',\omega-\omega')\,\mathrm{d}\omega'\,\mathrm{d}\boldsymbol{Q}'. \tag{21}$$

The resolution function was calculated from the instrumental parameters of our spectrometer by the method of Cooper and Nathans [27]. The correctness of these parameters was checked experimentally by scanning through the Bragg peaks of a perfect germanium crystal.

The differential cross section for the scattering of unpolarized neutrons from spin waves is given by [28]

$$\frac{\mathrm{d}^2\sigma}{\mathrm{d}\omega\,\mathrm{d}\Omega} = A(\boldsymbol{k}_i,\boldsymbol{k}_f)f^2(\boldsymbol{Q})\left(\frac{N\omega}{1-\mathrm{e}^{-\hbar\omega/kT}}\right)\chi^t(\boldsymbol{Q})F^t(\boldsymbol{Q},\omega) \tag{22}$$

where

$$\boldsymbol{Q} = \boldsymbol{k}_i - \boldsymbol{k}_f \qquad \hbar\omega = E_i - E_f\,.$$

Here k_i, E_i and k_f, E_f are the incident and scattered neutron wavevectors and energies, respectively, $f(Q)$ is the magnetic form factor, $\chi^t(Q)$ the transverse isothermal susceptibility of the system and $F^t(Q,\omega)$ the spectral weight function. As the functions $\chi^t(Q)$ and $F^t(Q,\omega)$ are periodic in Q-space, only their dependence on the reduced wavevector $q = Q - \tau$ will be considered in the following.

In the ferromagnetic regime at small q values, the q-dependent transverse susceptibility is $\chi^t(q) \sim q^{-2}$. Unfortunately, the theory does not predict the detailed shape of the spectral weight function $F^t(q,\omega)$. Two forms of this function are most commonly used. When the spin-wave interactions are negligible, $F^t(q,\omega)$ may be approximately written as the sum of two δ-functions

$$F^t(q,\omega) = \tfrac{1}{2}\big(\delta(\hbar\omega - \hbar\omega_q) + \delta(\hbar\omega + \hbar\omega_q)\big)\,. \tag{23}$$

If the effects of spin-wave interactions must be taken into account, the spectral weight function is usually approximated by a double Lorentzian

$$F^t(q,\omega) = \frac{1}{2\pi}\left(\frac{\Gamma}{(\hbar\omega - \hbar\omega_q)^2 + \Gamma^2} + \frac{\Gamma}{(\hbar\omega + \hbar\omega_q)^2 + \Gamma^2}\right) \tag{24}$$

where $\hbar\omega_q$ is the energy of the spin-wave with wavevector q, and Γ is energy linewidth of the spin wave.

In the data analysis we used both forms of $F^t(q,\omega)$, but much better fits were achieved with the Lorentzian lineshape. The observed spectrum at any wavevector and energy transfer was calculated as a four dimensional convolution of the assumed cross section with the instrumental resolution function by means of a computer program written originally at BNL [29]. The following parameters were fitted independently for each scan: the spin-wave stiffness constant D (assuming $\hbar\omega_q = Dq^2$), the linewidth $\Gamma(q)$, the peak intensity I and the background parameter B.

A difficult problem with the least-squares fitting of constant-E spectra is that the value of the stiffness constant D is highly correlated with the linewidth Γ, so that its fitted value depends on the form assumed for the damping. Among the physical processes leading to the finite spin-wave linewidth Γ, the main role should be played by magnon–magnon interactions and scattering of spin waves by magnetic impurities. The existing theories of spin-wave interactions in ferromagnets [30,31] predict the linewidth Γ to be, in the first approximation, proportional to q^4 for $\hbar\omega_q \ll kT$, while the theories of impurity scattering [32–34] give the spin-wave damping term proportional to q^5 or q^4 for small q. In the fitting procedure we have used both types of $\Gamma(q)$ dependence in the cross section given by (22) and (24). The quality of the fit and the obtained values of parameters were similar in both cases. Some additional fits with $\Gamma \sim q^2$ have also been performed to check the sensitivity of the obtained parameters on the assumed form of $\Gamma(q)$, but the quality of those fits was much worse than for $\Gamma \sim q^4$. Selected results of the fits of the Lorentzian cross section with $\Gamma(q) = Aq^4$ to the experimental data for room temperature are presented in table 4. The fitted peak intensity I and the background parameter B are scaled to the same number of monitor counts. The attached reduced χ^2 values describe the quality of the fit. The full curves in figure 5 represent the results of the fits.

For scans with $E > 10$ meV the procedure of simultaneous fitting of all parameters proved to be unstable because of the high background level and low statistics of the data. In this case the mean value of stiffness constant D obtained from scans with lower energy transfers was kept constant and only remaining parameters were fitted (see examples in table 4).

Table 4. Selected results of the fits of the Lorentzian cross section to spin-wave peaks measured by the constant-E method. D denotes the stiffness constant, $\Gamma = Aq^4$ the linewidth, I the intensity of magnon peak and B the background. In the measurements with $\lambda_f = 2.34$ Å the PG filter has been used.

E (meV)	λ_f (Å)	D (meV Å^2)	A (10^3 meV Å^4)	I	B	q (Å^{-1})	$\Gamma = Aq^4$ (meV)	χ^2
1	2.34	93(2)	3.80(17)	7.7(2)	102(2)	0.104(1)	0.4(1)	0.98
3	2.20	96(3)	1.41(12)	8.6(5)	34(1)	0.177(2)	1.4(2)	1.73
5	2.20	94(3)	0.87(5)	7.9(5)	24(1)	0.231(3)	2.5(2)	0.92
8	2.20	96(5)	0.57(6)	6.8(8)	26(1)	0.288(7)	4.0(6)	1.41
10	2.34	88(9)	0.54(7)	5.9(10)	10(1)	0.337(16)	7(2)	1.27
12	2.34	95 (fixed)	0.61(8)	4.5(5)	10(1)	0.355	10(2)	1.20
18	2.34	95 (fixed)	0.35(5)	7.9(11)	12(1)	0.435	12(2)	1.13

4.4. Discussion of results

The resulting spin-wave dispersion relation of the assumed quadratic form $\hbar\omega_q = Dq^2$ obtained after correction of all the data for the instrumental resolution function is shown in figure 6. The full curve corresponds to the mean value of $D_{RT} = 95 \pm 3$ meV Å^2 for scans with energy transfer $E \leq 10$ meV. The positions of the longitudinal (LA) and transverse (TA) acoustic phonon branches are also shown in figure 6.

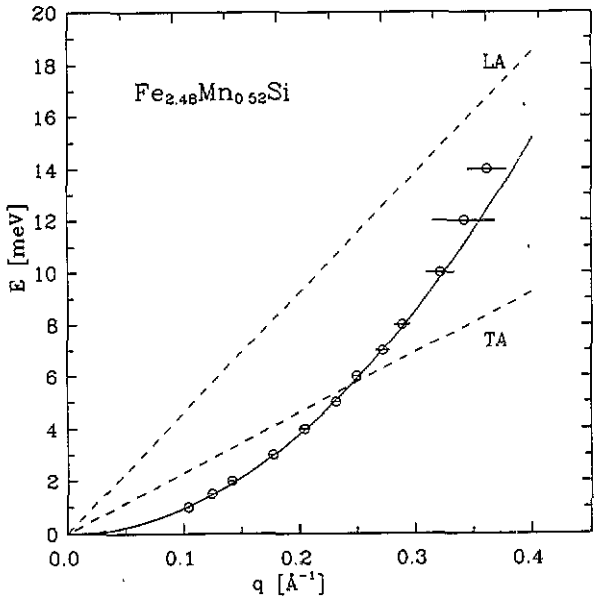

Figure 6. Spin-wave dispersion relation measured for $Fe_{2.48}Mn_{0.52}Si$ along the [111] direction at room temperature. *Points: experimental results corrected for experimental resolution;* full curve: quadratic relation with $D = 95$ meV Å^2.

As can be seen from table 4, there is a noticeable damping of the spin waves in our sample and the linewidth Γ is growing rather rapidly with magnon energy, nevertheless its q-dependence is weaker than $\Gamma = Aq^4$ assumed earlier in the fitting procedure. This

behaviour, manifesting itself by a significant decrease in the linewidth parameter, A, with increasing magnon energy, is in general agreement with the theoretical predictions of Brooks Harris [30]. His calculations for a simple cubic Heisenberg ferromagnet show that the interaction between spin waves leads to damping of the form

$$\Gamma = A_1 q^4 T^2 \left[\frac{1}{6}\ln^2\left(\frac{kT}{\hbar\omega_q}\right) + \frac{5}{9}\ln\left(\frac{kT}{\hbar\omega_q}\right) - 0.05\right] \qquad \text{for } \hbar\omega_q \ll kT \tag{25}$$

where A_1 is simply a coefficient of proportionality.

It can be seen from figure 7 that this form of damping fits our experimental data for the linewidth Γ much better than the simple q^4 or q^5 functional forms predicted by the theories of spin-wave scattering by magnetic impurities [32–34]. This, however, should not be understood as any strong indication that the magnon–magnon interaction is a dominant one. The Brooks Harris formula seems to work well, as in many other systems including amorphous ones. It should be noted that our data cover the region of intermediate rather than very small values of q, to which the theories of impurity scattering apply. More detailed discussion of this problem, including data obtained for other samples and temperatures, will be presented elsewhere.

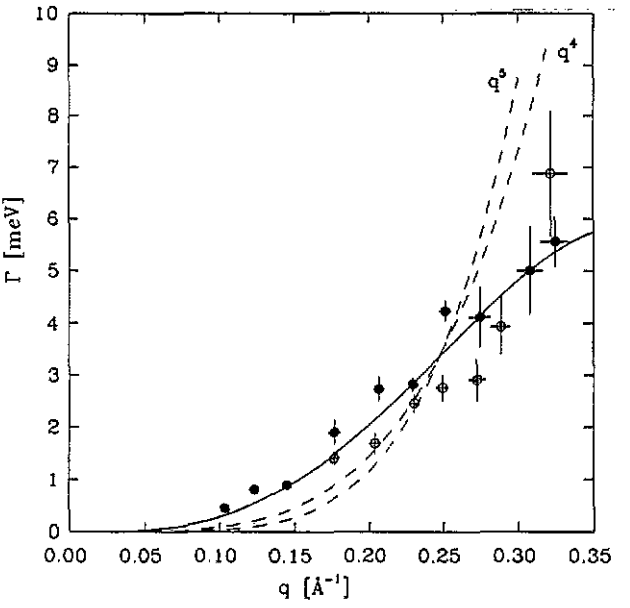

Figure 7. Magnon energy linewidth, Γ, determined from inelastic neutron scattering at room temperature. Full curve: fit to the theoretical function (25) of Brooks Harris [30]. Open and full circles correspond to measurements with $\lambda_f = 2.2$ Å and $\lambda_f = 2.34$ Å, respectively.

The numerical analysis of the data obtained at liquid-nitrogen temperature posed a more difficult problem, because of much lower statistics compared with the room-temperature data. The effects of the renormalization of spin-wave energies were clearly visible, but reliable results of the fits could only be achieved for scans with small energy transfers ($E \leq 5$ meV). Therefore the mean value of the stiffness constant at

Table 5. Stiffness constants, effective exchange integrals, Curie temperatures and spontaneous magnetizations of $Fe_{3-x}Mn_xSi$ alloys obtained from magnetic and neutron scattering studies. D_{LN} for Fe_3Si was estimated only (see text). Spontaneous magnetizations at 4.2 K are expressed as Bohr magnetons per formula unit.

x	D_{RT} (meV Å^2)	D_{LN} (meV Å^2)	J_{eff} (meV)	T_C (K)	μ (μ_B)
0	240 ± 10	240 ± 15	24.8 ± 1.0		
0.04	231 ± 3	235 ± 10	24.7 ± 1.0	838	4.92
0.18	173 ± 3	198 ± 5	22.4 ± 0.4	750	4.36
0.32	145 ± 3	159 ± 5	19.9 ± 0.4	655	4.10
0.52	95 ± 3	110 ± 10	16.9 ± 0.8	497	3.25

liquid-nitrogen temperature, $D_{LN} = 110 \pm 10$ meV Å^2, was obtained with a rather low precision.

In the course of the data analysis it became obvious that the fitted value of the stiffness constant D depends on the assumed form of the spin-wave damping. This suggested a need to re-analyse our earlier results with respect to the damping. Thus the Lorentzian form of the cross section (24) was also fitted to the results of our earlier measurements performed for alloys with lower manganese concentration at room temperature [2,4] as well as liquid-nitrogen temperature [25]. The values of stiffness constants $D_{RT}(x)$ and $D_{LN}(x)$ obtained are summarized in table 5 together with the value $D_{RT}(0)$ for pure Fe_3Si taken from [23].

As can be seen from table 5, the renormalization of the stiffness constant between liquid-nitrogen and room temperature is rather small for all the samples measured. This means that the value of stiffness constant determined at the liquid-nitrogen temperature may be treated as a good approximation of its value at 0 K and used for evaluation of exchange integrals. The stiffness constant for pure Fe_3Si was measured at room temperature only, but the data in table 5 for $Fe_{3-x}Mn_xSi$ alloys suggest no significant energy renormalization in Fe_3Si when the temperature is decreased from the room temperature ($0.36T_C$) to liquid-nitrogen temperature ($0.09T_C$). Therefore, in this case we increased the error of exchange stiffness constants to show the upper expected limit of D.

The Curie temperatures T_C determined for these alloys from the temperature dependence of the magnetization and from neutron diffraction measurements of the (111) magnetic reflection intensity are also shown in table 5. The Curie temperature decreases rather rapidly with growing manganese content in the alloy and, as mentioned before, it was used as an additional check on the composition of the samples. Table 5 also contains the results of our measurements of spontaneous magnetization at 4.2 K, which are in very good agreement with the values reported for the same alloys by Booth *et al* [7].

The final results of our analysis are the effective exchange integrals $J_{eff}(x)$ obtained from equation (12) for all measured compositions of the alloy. The magnetic moments of A and B sites were taken from [1] and the stiffness constants at 0 K were approximated by $D_{LN}(x)$.

5. Effective exchange integrals in the $Fe_{3-x}Mn_xSi$ system

The dependence of the effective exchange integrals J_{eff} on the sample composition can

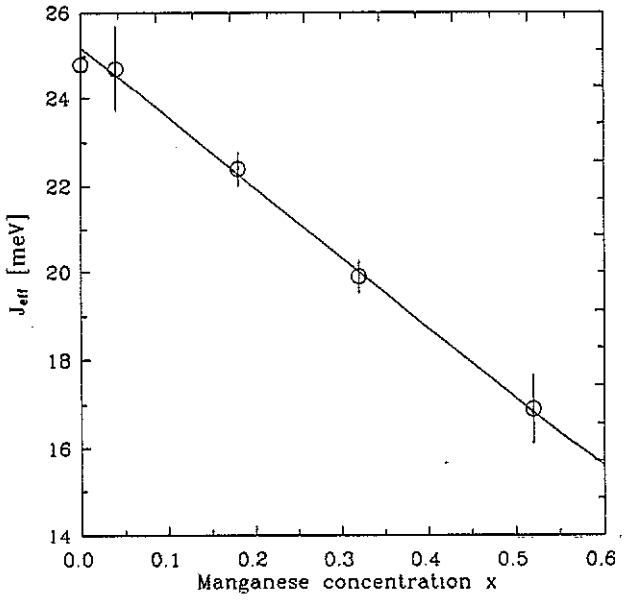

Figure 8. Concentration dependence of the effective exchange integral J_{eff} in ordered $Fe_{3-x}Mn_xSi$ alloys. The full line represents the fit of equation (16) with parameters given by (26).

be analysed now with the aid of (16). The least-squares fitting of this equation to the values of $J_{\text{eff}}(x)$ presented in table 5 gives (see figure 8)

$$\begin{aligned} J_{\text{eff}}(0) &= 25.4 \pm 0.8 \text{ meV} \\ J^{\text{eff}}_{\text{Fe-Mn}} &= 8.2 \pm 3.9 \text{ meV} \\ J^{\text{eff}}_{\text{Mn-Mn}} &= 0.2 \pm 1.2 \text{ meV}. \end{aligned} \tag{26}$$

These results differ from the first estimates published in [4], but apparently the weakness of the effective Mn–Mn interaction is confirmed. This can be interpreted as either a negligible Mn–Mn interaction or as indicating competition between $J_{\text{Mn-Mn}}(3)$ and $J_{\text{Mn-Mn}}(6)$ interactions. The latter hypothesis follows the idea of Ziebeck and Webster [35], which aimed to explain the antiferromagnetic component seen in neutron diffraction patterns of Fe_2MnSi. Nevertheless, with the set of exchange integrals (26) it is hard to explain the instability of the ferromagnetic state at $x = 0.75$.

We note that effective Fe–Mn interaction is roughly three times weaker than the exchange interactions between iron atoms. This can result in a greater sensitivity of the manganese magnetic moment to temperature than is the case for the iron moment. In fact, these were the expectations of Kępa and Hicks [13]. In particular, their estimate of μ_{Mn} is about $0.6\mu_{\text{B}}$ at room temperature, whereas all measurements [1,7,8,9] carried out at liquid-helium temperature indicated that the moment was close to $2.2\mu_{\text{B}}$.

Let us use (14) and (15) consistently but with S_{Mn} different from the average spin at B site. We then obtain

$$J_{\text{eff}} = (1-x)\left(\frac{S_{\text{Fe}B}}{\langle S_B\rangle}\right)J_{\text{eff}}(0) + x\left(\frac{S_{\text{Mn}}}{\langle S_B\rangle}\right)J^{\text{eff}}_{\text{Fe-Mn}} + \left(\frac{x^2}{1-x}\right)\left(\frac{2S^2_{\text{Mn}}}{S_A(0)\langle S_B\rangle}\right)J^{\text{eff}}_{\text{Mn-Mn}} \tag{27}$$

where $\langle S_B \rangle = (1-x)S_{FeB} + xS_{Mn}$.

The short-range ordering found by Kępa and Hicks [13] would add an extra term to (27), namely

$$2\alpha_1 x \frac{S_{FeB}^2 J_{FeB-FeB}(3) - S_{FeB}S_{Mn}J_{Fe-Mn}(3) + S_{Mn}^2 J_{Mn-Mn}(3)}{S_A(0)\,(S_{FeB} - x(S_{FeB} - S_{Mn}))} \tag{28}$$

where the short-range order parameter $\alpha_1 \approx 0.16$. In the case of $S_{Mn} = S_{FeB}$ this term reduces to

$$2\alpha_1 x \left(\frac{S_B}{S_A(0)}\right)\left(J_{FeB-FeB}(3) - J_{Fe-Mn}(3) + J_{Mn-Mn}(3)\right). \tag{29}$$

One can easily check that with $S_{FeB} = 1.1$ and $S_{Mn} \approx 0.3$ [13] the values of J_{eff} calculated from (27) using the parameters given by (26) would be considerably higher than the values obtained from our experiment performed at room temperature. For example, for $x = 0.32$ the calculated value is 23.4 meV, while the experimental one is only 20.6 meV.

The inclusion of the short-range ordering could even increase this difference, as the leading term in (28) is proportional to $J_{FeB-FeB}(3)$ when S_{Mn} is as small as 0.3. As can be seen from table 2, $J_{FeB-FeB}(3)$ is of the order of 2.5 meV, so we can expect that the term (28) will (for $x = 0.32$) be positive, although smaller than 1 meV. On the other hand, the correction to J_{eff} caused by the short-range order at low temperatures (where $S_{Mn} = S_{FeB}$) is given by (29) and does not exceed 0.5 meV for reasonable values of $J_{Fe-Mn}(3)$ and $J_{Mn-Mn}(3)$.

The difference between the calculated and experimental values of J_{eff} could probably be slightly reduced if the temperature spin-wave energy renormalization were taken into account. Nevertheless, one can say that our data, when analysed in terms of the Heisenberg model as described above, do not agree with the magnetic moment distribution found at room temperature by Kępa and Hicks [13]. This shows that much more subtle model of the spin dynamics should be worked out for this system.

In conclusion, we can state the following.

(i) From the spin-wave stiffness constants of $Fe_{3-x}Mn_xSi$ alloys, measured at low temperatures, the effective exchange integrals for the Fe–Fe, Fe–Mn and Mn–Mn can be estimated on the basis of the Heisenberg model. The estimated values are given by (26).

(ii) The effective Fe–Mn interaction is roughly one third of the Fe–Fe interaction. This is a much higher fraction than $J_{Fe-Mn}/J_{Fe-Fe} \approx 0.1$ estimated by Nakai and Kunitomi [10] for disordered Fe–Mn alloys. The latter value was used to explain a much more rapid decrease of the manganese magnetic moment with temperature than that for iron. In fact, a similar conclusion could be reached from the Kępa and Hicks estimate of S_{Mn} at room temperature. However, our results show that the relation between the variation with temperature of the magnetic moment and the exchange integrals between the nearest neighbours (or any kind of 'effective' interactions) is much more subtle.

(iii) The effective interactions between manganese atoms is found to be very weak. Even for the lowest acceptable value (within experimental error), about -1 meV, the instability of the ferromagnetic state can be expected for $x > 0.8$, while it is known that it appears at $x \approx 0.75$. Extensive investigations of the magnetic structure of

Fe_2MnSi at 4.2 K has lead Ziebeck and Webster [35] to conclude that 'the exchange interactions between second-neighbour Mn sites must be negative and be greater than the exchange between first neighbours'. It seems that, within the accuracy of the experiment, our results do not contradict this statement.

(iv) The effective exchange interactions J_{eff} are slightly smaller at room temperature than at low temperature. With the requirement that S_{Mn} be significantly reduced at room temperature, the simple 'average crystal' approximation fails to explain the observed values of J_{eff}, unless the exchange interactions themselves significantly renormalise with temperature.

Acknowledgments

The authors are grateful to Drs J B Forsyth and K R A Ziebeck for providing us with their experimental data on Fe_3Si.

This work was partly supported by the Polish Government under grant No CPBP 01.09.

Appendix A

The values of the coefficients in the Hamiltonian (4) for [100] direction are

$$a_1 = 8S_A\left[J_{AB}(1) + 3J_{AB}(4) + 3J_{AB}(7)\right] + 4S_B\left[4J_{BB}(3)\sin^2(ka/4) + J_{BB}(6)\sin^2(ka/2)\right] \tag{A1}$$

$$a_2 = 4S_B\left[J_{AB}(1) + 3J_{AB}(4) + 3J_{AB}(7)\right] + 4S_A\left[\left(J_{AA}(2) + 4J_{AA}(3) + 4J_{AA}(5) + 4J_{AA}(8)\right)\sin^2(ka/4) + \left(J_{AA}(6) + 4J_{AA}(8)\right)\sin^2(ka/2)\right] \tag{A2}$$

$$a_{12} = 8\sqrt{2S_AS_B}\left[J_{AB}(1)\cos(ka/4) + J_{AB}(4)\left(\cos(3ka/4) + 2\cos(ka/4)\right) + J_{AB}(7)\left(2\cos(3ka/4) + \cos(ka/4)\right)\right] \tag{A3}$$

$$a_3 = 8S_B\left[J_{AB}(1) + 3J_{AB}(4) + 3J_{AB}(7)\right] + 8S_A\left[J_{AA}(2)\left(3 - \sin^2(ka/4)\right) + 4J_{AA}(3)\sin^2(ka/4) + J_{AA}(6)\sin^2(ka/2) + 4J_{AA}(5)\cos^2(ka/4) + 2J_{AA}(8)\left(3 + 2\cos^2(ka/2) + \cos(ka/2)\right)\right] \tag{A4}$$

where $J_{\alpha\beta}(n)$ denotes the exchange integral between the nth nearest neighbours, one of which is located at the α site while the other resides at the β site.

For the [110] direction we have respectively

$$a_1 = 8S_A\left[J_{AB}(1) + 3J_{AB}(4) + 3J_{AB}(7)\right] + 4S_B\left[J_{BB}(3)\left(\sin^2(ka/2\sqrt{2}) + 4\sin^2(ka/4\sqrt{2})\right) + 2J_{BB}(6)\sin^2(ka/2\sqrt{2})\right] \tag{A5}$$

$$a_2 = 4S_B\left[J_{AB}(1) + 3J_{AB}(4) + 3J_{AB}(7)\right] + 4S_A\left[\left(2J_{AA}(2) + 4J_{AA}(3)\right)\sin^2(ka/4\sqrt{2}) + \left(J_{AA}(3) + 2J_{AA}(5) + 2J_{AA}(6)\right)\sin^2(ka/2\sqrt{2})\right.$$

$$+ 8J_{AA}(8)\left(1 - \cos^2(ka/2\sqrt{2})\cos^2(ka/4\sqrt{2})\right)] \tag{A6}$$

$$\begin{aligned} a_{12} = 8\sqrt{2S_AS_B}\,[&J_{AB}(1)\cos^2(ka/4\sqrt{2}) \\ &+ J_{AB}(4)\left(\cos^2(3ka/4\sqrt{2}) + 2\cos(3ka/4\sqrt{2})\cos(ka/4\sqrt{2})\right) \\ &+ J_{AB}(7)\left(\cos^2(3ka/4\sqrt{2}) + 2\cos(3ka/4\sqrt{2})\cos(ka/4\sqrt{2})\right)] \end{aligned} \tag{A7}$$

$$\begin{aligned} a_3 = 8S_B\left[J_{AB}(1) + 3J_{AB}(4) + 3J_{AB}(7)\right] + 8S_A\,[&J_{AA}(2)\left(2 + \cos(ka/2\sqrt{2})\right) \\ &+ 4J_{AA}(3)\sin^2(ka/4\sqrt{2})\left(1 + \cos^2(ka/4\sqrt{2})\right) \\ &+ 2J_{AA}(5)\left(1 + \cos^2(ka/2\sqrt{2})\right) + 2J_{AA}(6)\sin^2(ka/2\sqrt{2}) \\ &+ 4J_{AA}(8)\left(1 + 2\cos^2(ka/2\sqrt{2})\cos^2(ka/4\sqrt{2})\right)] \end{aligned} \tag{A8}$$

For the [111] direction, the coefficients in equation (9) are

$$\begin{aligned} a_{11} = 8S_B\left[J_{AB}(1) + 3J_{AB}(4) + 3J_{AB}(7)\right] + 4S_A\,[&3J_{AA}(2) + 4J_{AA}(5) \\ &+ 12J_{AA}(8) + 6\left(J_{AA}(3) + J_{AA}(6)\right)\sin^2(ka/2\sqrt{3})] \end{aligned} \tag{A9}$$

$$\begin{aligned} a_{12} = -2\sqrt{S_AS_B}\,[&J_{AB}(1)\left(e^{i(3ka/4\sqrt{3})} + 3e^{-i(ka/4\sqrt{3})}\right) \\ &+ 3J_{AB}(4)\left(2e^{i(3ka/4\sqrt{3})} + e^{-i(5ka/4\sqrt{3})} + e^{-i(3ka/4\sqrt{3})}\right) \\ &+ J_{AB}(7)\left(3e^{i(7ka/4\sqrt{3})} + 3e^{-i(5ka/4\sqrt{3})}\right. \\ &\left. + e^{i(5ka/4\sqrt{3})} + 4e^{-i(ka/4\sqrt{3})} + e^{i(ka/4\sqrt{3})}\right)] \end{aligned} \tag{A10}$$

$$\begin{aligned} a_{13} = -4S_A\,[&3J_{AA}(2)\cos(ka/2\sqrt{3}) + 4J_{AA}(5)\cos^3(ka/2\sqrt{3}) \\ &+ 12J_{AA}(8)\cos(ka/\sqrt{3})\cos(ka/2\sqrt{3})] \end{aligned} \tag{A11}$$

$$\begin{aligned} a_{22} = 16S_A\left[J_{AB}(1) + 3J_{AB}(4) + 3J_{AB}(7)\right] \\ + 24S_B\left[J_{BB}(3) + J_{BB}(6)\right]\sin^2(ka/2\sqrt{3})\,. \end{aligned} \tag{A12}$$

References

[1] Niculescu V A, Burch T J and Budnick J I 1983 *J. Magn. Magn. Mater.* **39** 223

[2] Dobrzyński L, Blinowski K, Bednarski S, Kępa H, Giebułtowicz T, Minor W, Krašnicki S, Kosiorowska J and Weiss L 1981 *Solid State Commun.* **38** 773

[3] Kępa H, Dobrzyński L, Wiśniewski A, Szymański M, Minor W, Piotrowski M and Blinowski K 1986 *Solid State Commun.* **57** 47

[4] Dobrzyński L 1987 *Proc. 4th School-Symp. Physics of Metals (Piechowice, 1987), Phys. Chem. Solids* (Wrocław: Institute of Low Temperature Physics) p 124

[5] Kajzar F and Parette G 1980 *Phys. Rev.* B **22** 5471

[6] Radakrishna P and Livet F 1978 *Solid State Commun.* **25** 597

[7] Booth J G, Clark J E, Ellis J D, Webster P J and Yoon S 1974 *Proc. Int. Conf. on Magnetism (Moscow, 1973)* **4** 577

[8] Yoon S and Booth J G 1974 *Phys. Lett.* **48A** 381
Yoon S 1975 *PhD Thesis* Salford University, UK

[9] Yoon S and Booth J G 1977 *J. Phys. F: Met. Phys.* **7** 1079

[10] Nakai Y and Kunitomi N 1975 *J. Phys. Soc. Japan* **39** 1257

[11] Mezei F 1976 *Proc. Conf. on Neutron Scattering (Gatlinburg)* ed R M Moon (Oak Ridge, TN: Oak Ridge National Laboratory) p 670

[12] Child H R and Cable J W 1976 *Phys. Rev.* B **13** 227

[13] Kępa H and Hicks T J 1988 *J. Physique Coll.* Suppl. 12 **49** C8 111
[14] Shull R D, Okamoto H and Beck P E 1976 *Solid State Commun.* **20** 863
[15] Motoya K, Shapiro S M and Muraoka Y 1983 *Phys. Rev.* B **28** 6183
[16] Huffman S P 1973 *Amorphous Magnetism* ed H O Hooper and A W Graaf (New York: Plenum) p 283
[17] Dobrzyński L, Giebułtowicz T, Kopcewicz M, Piotrowski M and Szymański K 1987 *Phys. Status Solidi* a **101** 567
[18] Dobrzyński L, Blinowski K, Bednarski S, Kępa H, Giebułtowicz T and Minor W 1983 *Solid State Commun.* **46** 217
[19] Dobrzyński L, Wiśniewski A, Uemura Y J, Shapiro S M and Wicksted J P 1988 *Phys. Rev.* B **37** 7175
[20] Leoni F and Natoli C 1969 *Physica* **40** 553
[21] Kawamiya N, Adachi K and Nakamura Y 1972 *J. Phys. Soc. Japan* **33** 1318
[22] Ziebeck K R A and Forsyth J B unpublished results
[23] v. Blanckenhagen P and Lin C 1981 *Physics of Transition Metals 1980 (Inst. Phys. Conf. Ser. 55)* ed P Rhodes (Bristol: Institute of Physics) p 371
[24] Caroli B and Blandin A 1966 *J. Phys. Chem. Solids* **27** 503
[25] Kępa H, Kłosowski P, Szymański M and Wiśniewski A 1985 unpublished
[26] Kępa H 1988 private communication
[27] Cooper M J and Nathans R 1967 *Acta Crystallogr.* **23** 357
[28] Marshall W and Lovesey S W 1971 *Theory of Thermal Neutron Scattering* (Oxford: Clarendon)
[29] Heilmann I U and Tarvin J A 1978 unpublished
[30] Brooks Harris A 1968 *Phys. Rev.* **175** 674
[31] Vaks V G, Larkin A I and Pikin S A 1968 *Zh. Eksp. Teor. Fiz.* **26** 647
[32] Callaway J 1963 *Phys. Rev.* **132** 2003
[33] Murray G A 1966 *Proc. Phys. Soc.* **89** 87
[34] Singh A and Tesanović Z 1989 *Phys. Rev.* **B39** 7284
[35] Ziebeck K R A and Webster P J 1976 *Phil. Mag* **34** 973